

A 12-years long (2010-2021) hydrological and biogeochemical dataset in the Sicily Channel (Mediterranean Sea)

Francesco Placenti¹, Marco Torri^{2*}, Katrin Schroeder³, Mireno Borghini⁴, Gabriella Cerrati⁵, Angela Cuttitta², Vincenzo Tancredi¹, Carmelo Buscaino¹, Bernardo Patti⁶

¹Consiglio Nazionale delle Ricerche - Istituto per lo studio degli impatti Antropici e Sostenibilità in ambiente marino (CNR-IAS), Campobello di Mazara (TP), Italy.

²Consiglio Nazionale delle Ricerche – Istituto di Studi sul Mediterraneo (CNR-ISMed), Palermo, Italy.

³Consiglio Nazionale delle Ricerche – Istituto di Scienze Marine (CNR-ISMAR), Venice, Italy.

⁴Consiglio Nazionale delle Ricerche – Istituto di Scienze Marine (CNR-ISMAR), La Spezia, Italy

⁵ENEA – Infrastrutture e Servizi – Servizio e Gestioni Centro Santa Teresa (ISER-STE), Santa Teresa, La Spezia, Italy;

⁶Consiglio Nazionale delle Ricerche - Istituto per lo studio degli impatti Antropici e Sostenibilità in ambiente marino (CNR-IAS), Palermo, Italy.

*Corresponding author: marco.torri@cnr.it

ABSTRACT

1 The data set presented here consists of 273 Conductivity-Temperature-Depth (CTD) stations, as well
2 as 2034 sampled data points in the water column, where dissolved inorganic nutrients have been
3 measured, that were collected during 12 summer oceanographic cruises (BANSIC series) in the Sicily
4 Channel (Central Mediterranean Sea), between 2010 and 2021. The quality of the CTD dataset is
5 ensured by regular sensor calibrations, an accurate control process adopted during the acquisition,
6 processing and post-processing phases. The quality of the biogeochemical dataset is ensured by the
7 adoption to best-practices analytical and sampling methods. This data collection fills up a gap of
8 information in the Sicily Channel, i.e. a key area where complex water mass exchange processes
9 involve the transfer of physical and biogeochemical properties between the Eastern and the
10 Western Mediterranean. The available dataset will be useful to evaluate the long-term variability
11 on a wide spatial scale, supporting studies on the evolution of the Mediterranean circulation and its
12 peculiar biogeochemistry, as well as on the physical and biogeochemical modeling of this area.

13

14 INTRODUCTION

15 The thermohaline circulation in the Mediterranean Sea (MS) is anti-estuarine and is driven by the
16 negative freshwater budget and the net heat loss over the whole basin. The Mediterranean
17 thermohaline circulation drives the transport of water masses and biogeochemical elements in the

18 different basins (eastern and western) and, via the Strait of Gibraltar, controls the exchanges with
19 the Atlantic Ocean (The MerMex Group, 2011).

20 The Sicily Channel (SC), due to its particular bathymetric structure and geographic position, also
21 plays a key role in modulating the eastward transport of the fresher and superficial Atlantic Water
22 (AW) and the underlying westward transport of the salty Intermediate Water (IW) which forms in
23 the Eastern Mediterranean, called Levantine Intermediate Water (LIW) or Cretan Intermediate
24 Water (CIW), depending on the specific formation location (Levantine or Cretan Sea) (Schroeder et
25 al., 2017). From its formation area IW spreads westward into the Ionian Sea (IS), with a significant
26 flow northward towards the Adriatic Sea, where it constitutes an important preconditioning agent
27 for the formation of the Adriatic Deep Water (which forms the bulk of the Eastern Mediterranean
28 Deep Water, e.g. Gačić et al., 2013). When reaching the Western Mediterranean, and in particular
29 its northern part, the IW preconditions the water column also there and makes it prone to the
30 formation of Western Mediterranean Deep Water (e.g., Roether et al., 1996). Although the area of
31 the SC is limited at the east and west by two relatively shallow sills (max depths of 350 m and 550
32 m, respectively), in its central part the bottom depth can reach 1700 m. It is in this deep central
33 trench where e.g., Gasparini et al. (2005) and others studied the evolution of the upper part of the
34 Eastern Mediterranean Deep Water (or transitional Eastern Mediterranean Deep Water) over time,
35 being able to cross the SC and reach the Tyrrhenian Sea along with the IW flow. Several authors,
36 analyzing long time series of temperature and salinity of the deeper waters of the SC, have
37 highlighted a general positive trend albeit characterized by phases of accelerations and multiannual
38 peaks and fluctuations (Gasparini et al., 2005; Gačić et al., 2013; Bonanno et al., 2014; Ben Ismail et
39 al., 2014; Schroeder et al., 2017; Placenti et al., 2022). Furthermore, these trends are significantly
40 faster than those reported for the global ocean intermediate layer (Borghini et al., 2014; Schroeder
41 et al., 2017). In fact, the semi-enclosed nature of the MS, together with its smaller inertia due to the
42 relative short residence time of its water masses, makes it more sensitive to natural variations in
43 fluxes (between, e.g., the air and sea, freshwater and the sea) and water flows, identifying it as a
44 "hotspot" for climate change. Consequently, MS is expected to experience environmental impacts
45 that are considerably greater than those in many other places around the world (The MerMex
46 Group, 2011). As regards the peaks, trends and multiannual fluctuations of temperature and salinity
47 observed in the deeper water of the SC, they are probably ascribable to different processes acting
48 at different spatial and temporal scales, such as the passage of the signature of the Eastern
49 Mediterranean Transient (EMT) (Gasparini et al., 2005), the alternation of circulation phases

50 (cyclonic-anticyclonic) of the Northern Ionian Gyre (NIG) (Gačić et al., 2013; Bonanno et al., 2014;
51 Placenti et al., 2022) and the effects related to warming of the Eastern Mediterranean (Schroeder
52 et al. al., 2017, 2019).

53 The anti-estuarine circulation, jointly to the superposition of different time scales of variability,
54 intense wintertime atmospheric forcings, NIG reversals and EMT, act also on the distribution of
55 biogeochemical elements (e.g., inorganic nutrients) and productivity of the MS. The very low
56 productivity of the MS is therefore mainly linked both to the anti-estuarine circulation (Krom et al.,
57 2010) and to the chemical speciation of the dissolved P and N. They in fact reflect a switch from less
58 bioavailable chemical forms of P and N entering the Mediterranean Sea to more bioavailable forms
59 leaving it (Powley et al., 2017). Moreover, the export of nutrients through the IW causes the deep
60 waters of the Eastern Mediterranean Sea to be more nutrient depleted than deep water in all other
61 parts of the global ocean (Krom et al., 2005). Another peculiarity still debated is the higher molar
62 $\text{NO}_3:\text{PO}_4$ ratio in the deeper water of the MS compared to the “classical” world oceans Redfield
63 ratio, indicating a general P-limited regime, which becomes stronger along a west-to-east gradient
64 (Belgacem et al., 2020). In this context, the aim of this paper is to compile a large dataset of
65 hydrological (temperature, salinity and pressure) and biogeochemical (nitrate, phosphate and
66 silicate) properties from *in situ* data collected between 2010 and 2021 in the SC, filling up a gap of
67 information in a key area of the MS, where the exchange between the two basins is taking place.
68 The available dataset is a valuable tool in support to the evaluation of the long-term variability and
69 evolution of the Mediterranean circulation and water masses, and provides also a useful
70 contribution for the implementation of models aimed at describing the physical-chemical processes
71 occurring in this area. The dataset could also be integrated in the recently published climatology of
72 dissolved inorganic nutrients (Belgacem et al., 2020), to expand its geographic domain.

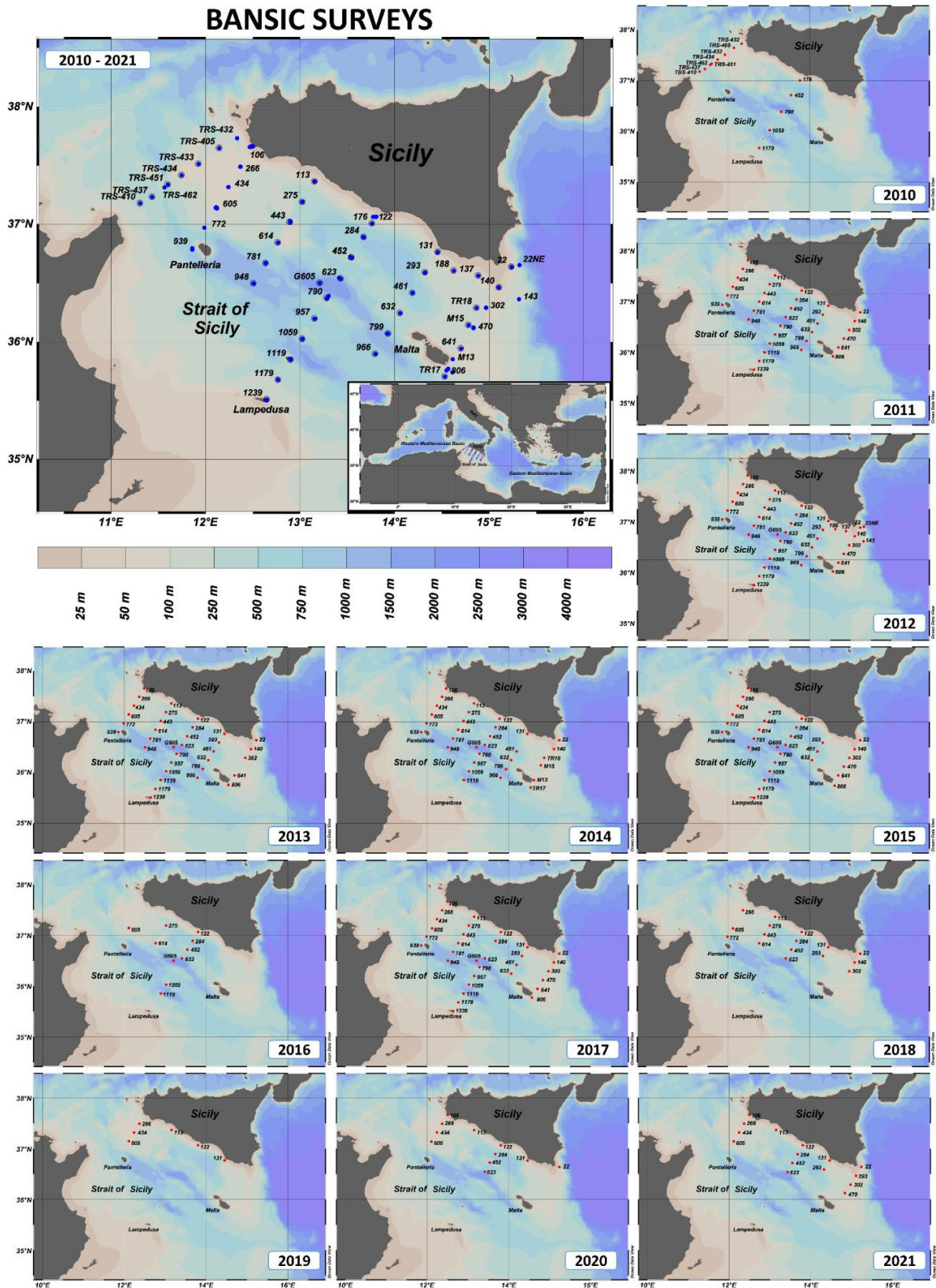
73

74 **DATASET AND METHODS**

75 The hydrological and biogeochemical data collection was carried out as part of an ichthyoplankton
76 monitoring and research program implemented by the Italian National Research Council (CNR). This
77 program was set up with the primary purpose of monitoring the spatio-temporal distribution of the
78 early life stages of European anchovy (*Engraulis encrasicolus*) in the SC and of studying its
79 relationship with the environmental variables, in support to the sustainable exploitation of the
80 population by local fisheries. In this context, since 1998 ichthyoplankton oceanographic surveys
81 based on a common sampling grid have been annually carried out during the summer period in the

82 SC, within the FAO Geographic Sub-Areas (GSAs) 13, 15 and 16. Since 2010, in addition to the meso-
83 zooplankton sampling, water sampling for the quantification of macro-nutrients has been included
84 in the survey work plan in order to better characterize the biogeochemical characteristics of the
85 water column and study the relationships with the biotic component.

86 The dataset presented here results from this sampling effort and assembles information from 12
87 summer oceanographic cruises conducted on board of different research vessels from 2010 to 2021
88 (R/V “Urania” from 2010 to 2014; R/V “Minerva Uno” from 2015 to 2017; R/V “G. Dallaporta” from
89 2018 to 2021). Data were integrated into a dataset consisting of 273 CTD-nutrient stations and 2034
90 data points (Suppl. 1). The stations are arranged along inshore-offshore transects approximately sub
91 perpendicular to the Sicilian coast, aiming at characterizing the oceanographic and biogeochemical
92 features in a key area for the understanding of the complex exchange processes between the
93 Eastern and Western basins (Fig. 1).



94

95 *Figure 1. Stations map of the BANSIC cruises, carried out in the Sicily Channel or Strait of Sicily from*
 96 *2010 to 2021: CTD and nutrient stations are indicated by blue (in the general map) and red circles*
 97 *(in the yearly maps). The maps were created using Ocean Data View software (<https://odv.awi.de/>).*

98 **Hydrological Data Acquisition**

99 At all stations, pressure, salinity, and temperature were measured with a CTD (conductivity,
100 temperature, and depth) probe (Sea-Bird Scientific) mod. SBE 911plus and a General Oceanics
101 rosette with 24 Niskin bottles of 12 L capacity. Temperature measurements were performed with a
102 SBE-3/F thermometer, with a resolution of 0.00015 °C/bit at -1 °C or 0.00018 °C/bit at 31 °C, and
103 accuracy of ±0.001 °C. The conductivity measurements were performed with a SBE-4C sensor, with
104 a resolution of 0.00004 S/m and accuracy of 0.0003 S/m, while for the salinity the accuracy is 0.002.
105 The vertical profiles of all parameters were obtained by sampling the signals at 24 Hz, with the
106 CTD/rosette going down at a speed of 1 m/s. The rosette is equipped with a sonar altimeter which
107 intercept the bottom 100-70 meters before getting to it. The altimeter is used just for safety, to
108 avoid the rosette to touch the bottom.

109

110 **Inorganic Nutrient Data Collection**

111 Seawater samples for dissolved inorganic nutrient analysis were collected from the surface to the
112 bottom by means of Niskin bottles. In particular, during the CTD upcast, a variable number of water
113 samples, at selected standard depth, has been considered (surface–25m–50m–75m–100m–150m–
114 200m–300m–400m–500m–600m–700m–800m–900m–1000m–bottom) with slight modifications
115 in the upper layer where significant hydrological variability is typical to occur. All materials used for
116 water sampling on board were earlier conditioned with 10% HCl and rinsed 3 times with ultrapure
117 water. Unfiltered samples were stored on board at –20°C.

118

119 **Analytical Methods for Inorganic Nutrients**

120 For all cruises, nutrient determination (nitrate, silicate, and phosphate) was carried out following
121 standard colorimetric methods of seawater analysis, defined by Grasshoff et al. (1999) and Hansen
122 and Koroleff (1999) adapted to an automated system. Specifically, the determination of phosphate
123 is based on the colorimetric method, in which a blue color is formed by the reaction of phosphate,
124 molybdate ion and antimony ion, followed by reduction with ascorbic acid. The reduced blue
125 phospho-molybdenum complex is read at 880 nm. Inorganic nitrate is reduced to nitrite at pH 8 in
126 a copperized cadmium reduction coil that reacts with an aromatic amine, leading to the final
127 formation of the azo dye measured at 550 nm. Then, the nitrite that is separately determined must
128 be subtracted from the total amount measured to get the nitrate concentration only. The

129 determination of soluble silicates is based on the reduction of a silico-molybdate complex in acid
130 solution to molybdenum blue by ascorbic acid and the absorbance is measured at 820 nm.

131 All the analysis of dissolved inorganic nutrients were carried out immediately after each
132 oceanographic cruise, in the nutrient laboratory of the Institute for the Study of Anthropic Impacts
133 and Sustainability in the Marine Environment (CNR-IAS) of Capo Granitola, using the same analytical
134 instrument and the same scientific staff. The concentration ($\mu\text{mol/l}$) of nitrate, silicate and
135 phosphate was measured by means of a Sial Autoanalyzer "QUAATRO". The detection limits for
136 nitrates, silicates and phosphates were 0.02, 0.01 and 0.006 $\mu\text{mol/l}$, respectively. Even though the
137 use of the same analytical methods, instruments and scientific staff supports the repeatability and
138 the comparison of the measurements, in order to further validate the analytical data, selected
139 seawater samples (sampled in duplicate) have been sent to the nutrient laboratory of nutrients of
140 the Research Center (ENEA) of Santa Teresa (La Spezia), taking advantage on their participation in
141 the framework of the European intercalibration program QUASIMEME (Quality Assurance of
142 Information for Marine Environmental Monitoring in Europe).

143 The differences in concentrations for all parameters analyzed (nitrates, phosphates and silicates)
144 ranged from 3% to 20%. The differences were greater (10-20%) for concentration values close to
145 the instrumental detection limit and smaller (<10%) at high concentrations. This range of differences
146 is perfectly acceptable considering that ENEA uses a previous generation auto-analyser and that the
147 scientific staff was different. However, we would like to point out that, in both nutrient laboratories,
148 the chemical analyzes were carried out using both the same analytical methods and the same types
149 of reagents.

150

151 **Quality check of hydrological and nutrient data**

152 The temperature and salinity of the CTD have been regularly calibrated. During 2 cruises, also
153 redundant temperature and salinity sensors were used. When they were available, the secondary
154 sensors have been used to assess the stability of the primary ones.

155 The temperature and salinity sensors calibrations have been performed before each cruise by CNR
156 technicians at the NATO Centre for Underwater Research (NURC, now Centre for Maritime Research
157 and Experimentation, CMRE) in La Spezia (Italy) until 2016. Between 2017 and 2018 sensors were
158 send to the manufacturer, while since 2019 the calibration is done at the new CNR-ISMAR
159 calibration laboratory in La Spezia (Italy). Table 1 shows a summary of all sensors, their serial
160 numbers and their calibration dates.

161 *Table 1. Calibration dates and serial numbers of the CTD sensors used during oceanographic cruises.*

Cruise	Date	Temp 1		Cond 1		Temp 2		Cond 2	
		sn	cal. date	sn	cal. date	sn	cal. date	sn	cal. date
Bansic 2010	25 Jun–14 Jul 2010	1368	May10	891	May10				
Bansic 2011	08–26 Jul 2011	4440	Apr11	3172	Apr11				
Bansic 2012	04–23 Jul 2012	1183	Nov10	923	Nov10				
Bansic 2013	26 Jun–16 Jul 2013	2810	Oct12	2483	Oct12				
Bansic 2014	22 Jul–9 Aug 2014	4440	Nov13	3172	Nov13				
Bansic 2015	16 Jul–3 Aug 2015	5022	Oct14	3485	Nov14				
Bansic 2016	30 Jun–14 Jul 2016	5022	Oct14	3485	Nov14				
Bansic 2017	13–29 Jun 2017	1183	Jul16	0923	Jun16				
Bansic 2018	07-19 Sep 2018	1142	Aug17	2779	Aug17				
Bansic 2019	30 Sep-12 Oct 2019	1142	Aug17	2779	Feb19	5038	May17	3484	Feb19
Bansic 2020	16-25 Sep 2020	1142	Jan20	2779	Jan20	5038	Jan20	3484	Jan20
Bansic 2021	6-18 Sep 2021	1381	Jun21	1048	Jun21				

162

163 After their acquisition, CTD data were pre-processed by the SBE Data Processing™ software, in order
 164 to (i) convert the raw data (.hex) to engineering units and store them in a text file (.cnv) (ii) run a
 165 low-pass filter on the data and smooth high frequency data, (iii) align parameter data in time,
 166 relative to pressure (to ensure that calculations of salinity and other parameters are made using
 167 measurements from the same parcel of water), (iv) remove conductivity cell thermal mass effects
 168 from the measured conductivity, (v) compute derived variables, and to (vi) average data, using
 169 averaging intervals based on depth range, and split the file into an upcast and a downcast file.

170 Following the recommendations of the SeaDataNet QC guidelines (SeaDataNet, 2010). The
 171 subsequent procedure to assess data quality was based on the following list:

- 172 - Check header details (vessel, cruise number, station numbers, date/time, latitude/longitude
 173 (start and end), instrument number and type, station depth, cast (up or down)), data
 174 type/no. of data points)
- 175 - Plot station positions to check not on land
- 176 - Check ship speed between stations to look for incorrect position or date/time
- 177 - Automatic range checking of each parameter
- 178 - Check units of parameters supplied
- 179 - Check pressure increasing
- 180 - Check no data points below bottom depth
- 181 - Plot profiles (individually, in groups, etc)
- 182 - Check for spikes
- 183 - Check for vertical stability/inversions
- 184 - Plot temperature vs. salinity

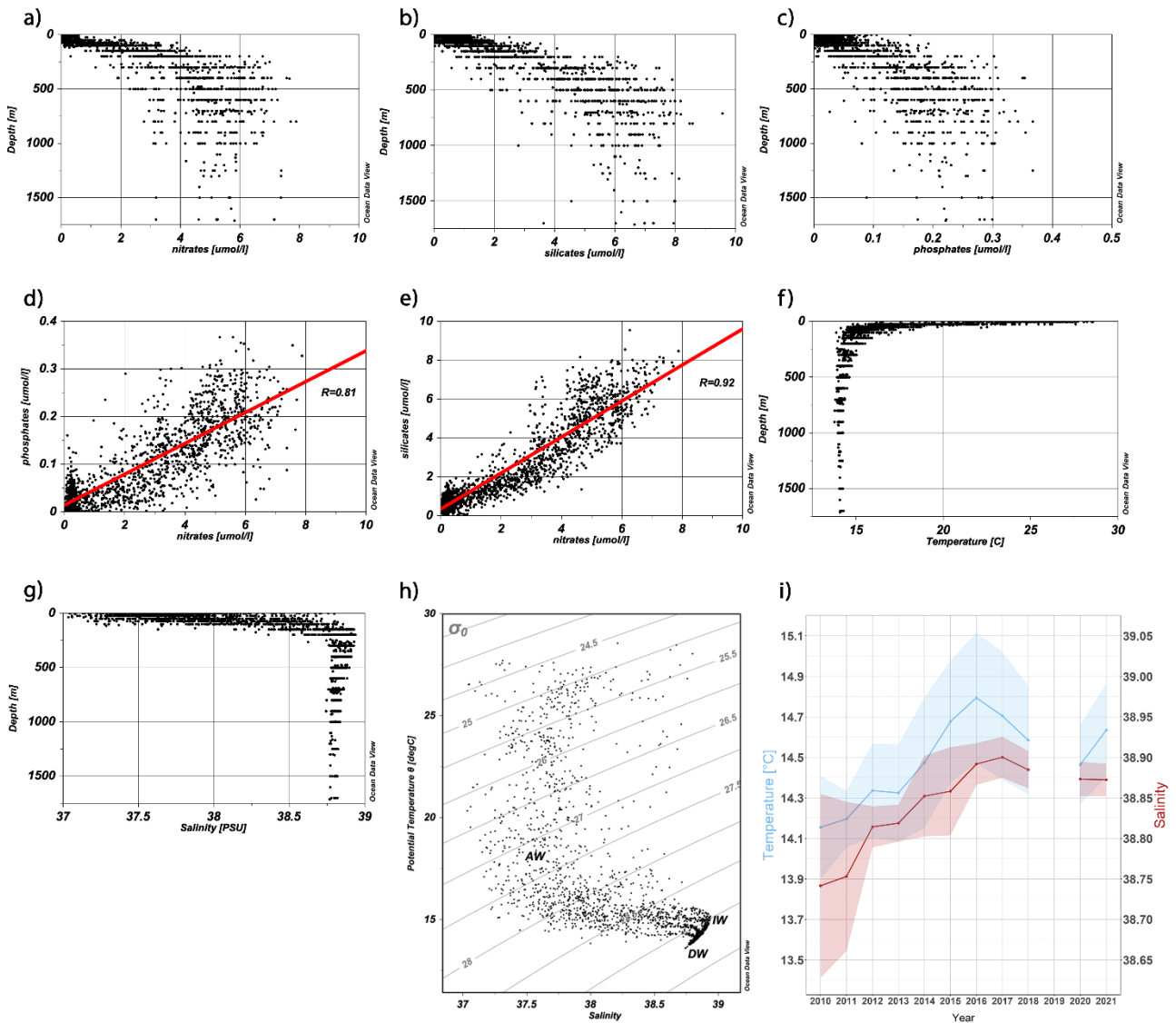
185 After the data acquisition, a post-processing control has been applied to the hydrological and
186 nutrient data acquired in the single survey as follow. After an initial visual inspection aimed at
187 removing any spike from the data profiles, an automatic control was carried out in R environment
188 in order to identify potential outliers. In particular, taking into account three layers (0-150 m, 151-
189 500 m and >500 m), potential outliers have been defined as values falling outside the range $\text{mean} \pm$
190 $3 \times \text{standard deviation}$ calculated in the relevant layer. Then, each potential outlier has been visually
191 double-checked within the recorded profiles in order to be validated or eliminated from the dataset.
192 Finally, with the aim at evaluating the consistency of the dataset collected in the 2010-2021 annual
193 surveys and performing a comparative control of the occurring patterns among years, the mean
194 value and the coefficient of variation (CV), i.e., a normalized measure of the dispersion given by the
195 ratio of the standard deviation to the mean, of hydrological and nutrient parameters were
196 calculated separately for each survey and for every identified water mass (Tab. 2). In this context,
197 based on the annual θ -S diagrams (as whole reported in Fig. 2h), three water masses were identified
198 in the study area and schematized below a surface layer of approximately 150 meters thick, variable
199 over the years and occupied mainly by AW, an intermediate layer (200-500 m) mainly occupied by
200 IW and a deeper layer (>500 m) occupied by the upper part of the deep water (DW).

201

202

203 **RESULTS AND DISCUSSION**

204 An analysis was conducted in order to characterize the spatial-temporal trends emerging in the
205 dataset and compare them with the state of the art concerning the study area. In this framework,
206 the vertical distribution pattern of inorganic nutrients in the water column of the SC highlights low
207 concentration values and high variability (Fig. 2; Tab. 2).



208
 209 *Figure 2. Plots of data on nutrients concentration at selected standard depths along the water*
 210 *column for a) nitrates, b) silicates, c) phosphates; d) N:P and e) N:Si diagrams and related linear*
 211 *regression lines (in red); f) plots of hydrological data at selected standard depths along the water*
 212 *column for temperature and g) salinity; h) potential temperature vs salinity diagram related to 2010-*
 213 *2021 period (AW for Atlantic Water, IW for Intermediate Water and DW for upper Deep Water) and*
 214 *i) time series of annual average values (2010-2021) of temperature (blue line) and salinity (red line)*
 215 *related to the water sampling depths in the IW (200-500 m). The related colored areas represent the*
 216 *standard deviations.*

217
 218 In surface waters the concentration values of inorganic nutrients are close to the instrumental
 219 detection limits due to the typical consumption of phytoplankton during the summer period
 220 occurring in this layer. This usually results in considerably lower values compared to patterns

221 observed in the underlying layers (Tab. 2). Moreover, the depth layer 0-150m is characterized by a
222 higher CV due to the pronounced dynamism of the exchange processes affecting the marine
223 ecosystem in this upper part of the water column as well as the interaction with terrestrial sources
224 of nutrients. Specifically, the lowest mean nitrate concentration value of 0.302 $\mu\text{mol/l}$ was
225 measured in BANSIC19 survey, characterized by a quite low number of water samples collected from
226 continental shelf stations only (no data of the intermediate layer are available from 2019 survey),
227 while the highest concentration value of 1.027 $\mu\text{mol/l}$ was measured in BANSIC14 survey (Tab. 2).
228 Regarding the phosphates the lowest mean concentration value was 0.030 $\mu\text{mol/l}$ (BANSIC12) and
229 the highest one 0.064 $\mu\text{mol/l}$ (BANSIC13), while for silicates the mean concentration values ranged
230 from a minimum of 0.608 $\mu\text{mol/l}$ (BANSIC15) to a maximum of 1.173 $\mu\text{mol/l}$ (BANSIC10) (Tab. 2).
231 The lower sampling effort carried out in BANSIC19 also corresponds to a lower variation of nitrates
232 and phosphates compared to the other surveys, while the silicates showed more homogeneous
233 patterns among surveys. Specifically, in the superficial layer CV varied between 0.762 (BANSIC19)
234 and 1.566 (BANSIC20) for nitrates, between 0.471 (BANSIC19) and 1.333 (BANSIC21) for phosphates,
235 and finally between 0.433 (BANSIC20) and 0.83 (BANSIC15) for silicates.

236 The inorganic nutrients are continuously consumed by phytoplankton at the sea surface and
237 regenerated in the mesopelagic layer by bacteria, increasing the nutrient concentrations in the
238 deeper water masses over time (e.g., Belgacem et al., 2020). In this way, the intermediate waters of
239 the SC are characterized by higher nutrient concentration values than the overlying layer and lower
240 variability (Fig. 2a-c and Tab. 2). Specifically, mean concentration values in the intermediate waters
241 ranged from 2.976 $\mu\text{mol/l}$ in BANSIC15 to 5.4 $\mu\text{mol/l}$ in BANSIC11 for nitrates, from 2.589 $\mu\text{mol/l}$
242 (BANSIC15) to 4.86 $\mu\text{mol/l}$ (BANSIC11) for silicates, and from 0.095 $\mu\text{mol/l}$ in BANSIC18 to 0.204
243 $\mu\text{mol/l}$ in 2021 for phosphates (Tab. 2).

244 Regarding the dispersion of the values in this layer, nitrates CV ranged between 0.068 (BANSIC20)
245 and 0.402 (BANSIC15), phosphates CV ranged between 0.171 (BANSIC20) and 0.585 (BANSIC16),
246 and silicates CV ranged between 0.161 (BANSIC20) and 0.528 (BANSIC15) (Tab. 2).

247 In the trench of the SC, the deep layer (see section >500m-bottom of Tab. 2) is characterized by
248 mean concentration values more homogeneous over years than in the above layers. There, the
249 lowest mean concentration values for nitrates and silicates (4.13 and 4.701 $\mu\text{mol/l}$) were measured
250 in BANSIC15, while the lowest value for phosphates (0.097 $\mu\text{mol/l}$) was measured during BANSIC10.
251 The highest mean values of nitrates (5.861 $\mu\text{mol/l}$), phosphates (0.241 $\mu\text{mol/l}$) and silicates (6.474
252 $\mu\text{mol/l}$) were respectively measured during BANSIC11, BANSIC17-21 and BANSIC13. Similarly, the

253 deep layer is characterized by the lowest variability in nutrient concentrations. Indeed, the nitrate
 254 CV varied between 0.0058 (BANSIC10) and 0.299 (BANSIC21), between 0.07 (BANSIC20) and 0.339
 255 (BANSIC10) for the phosphates and between 0.029 (BANSIC20) and 0.277 (BANSIC15) for the
 256 silicates.

257 The molar ratios of nitrate:phosphate (N:P) and silicate:nitrate (Si:N) in the whole water column of
 258 the SC show high correlation coefficients ($R=0.81$ and 0.92 , respectively) (Fig. 2d,e). Specifically, in
 259 the surface layer (0-150m) the mean values of N:P and Si:N over the period 2010-2021 are equal to
 260 18 and 1.4 respectively, which become 31 and 0.9 in the intermediate layer (200-500m) and 29 and
 261 1.1 in the deep layer (500m-bottom), in agreement with Ribera D'Alcalà et al. (2003) and with
 262 Placenti et al. (2013; 2022). Observed N:P values are higher than the classical Redfield ratio (16:1).
 263 The high N:P ratio can result from either a decrease in phosphate or an increase in nitrate; however,
 264 the reason of this anomaly is still unclear (e.g., Schroeder et al., 2010). Among the various
 265 hypotheses, we agree about the possible role of external inputs, together with very limited
 266 denitrification (Krom et al., 2010; Huertas et al., 2012; Van Cappellen et al., 2014), in explaining the
 267 observed very high $\text{NO}_3:\text{PO}_4$ ratios in the deeper water (Powley et al., 2017).

268

269 *Table 2. Average values of concentration and coefficients of variation (CV) of both physical*
 270 *(temperature and salinity) and chemical (nitrates, phosphates and silicates) parameters in the 12*
 271 *oceanographic surveys carried out yearly over the period 2010-2021 reported in this paper, by depth*
 272 *layer (superficial 0-150m, intermediate 200-500m and deep >500m-bottom).*

273

Cruise name	Sampling date	Research vessel name	Station number	Max. Sampling depth [m]	Sample number	Nitrates		Phosphates		Silicates		Temperature		Salinity	
						mean [$\mu\text{mol/l}$]	CV	mean [$\mu\text{mol/l}$]	CV	mean [$\mu\text{mol/l}$]	CV	mean [$^{\circ}\text{C}$]	CV	mean [psu]	CV
Layer 0-150 m															
Bansic10	25 June–14 Jul 2010	Urania	13	700	62	0.743	1.172	0.043	1.009	1.173	0.697	17.477	0.148	37.610	0.011
Bansic11	08–26 Jul 2011	Urania	34	1130	154	0.736	1.446	0.034	0.831	1.002	0.686	18.574	0.234	37.978	0.0087
Bansic12	04–23 Jul 2012	Urania	39	1711	203	0.707	1.066	0.030	0.954	1.037	0.478	17.923	0.237	38.177	0.0117
Bansic13	26 June–16 Jul 2013	Urania	34	1700	178	0.835	1.302	0.064	0.727	1.061	0.628	17.380	0.175	37.919	0.0094
Bansic14	22 Jul–9 Aug 2014	Urania	32	1700	164	1.027	1.116	0.051	0.803	0.940	0.703	17.997	0.201	37.872	0.0123
Bansic15	16 Jul–3 Aug 2015	Minerva Uno	31	1700	158	0.681	1.117	0.036	0.893	0.608	0.833	18.313	0.240	38.206	0.0093
Bansic16	30 June–14 Jul 2016	Minerva Uno	10	1700	51	0.777	1.237	0.043	0.638	0.614	0.690	17.673	0.176	37.812	0.0135
Bansic17	13–29 June 2017	Minerva Uno	32	1700	160	0.898	1.015	0.037	1.037	1.043	0.538	17.880	0.179	37.956	0.0125
Bansic18	07-19 Sept 2018	G. Dallaporta	16	700	77	0.957	1.286	0.039	0.671	1.150	0.649	18.646	0.229	38.091	0.0118
Bansic19	30 Sept-12 Oct 2019	G. Dallaporta	6	72	21	0.302	0.762	0.040	0.471	0.721	0.605	19.784	0.189	38.037	0.0068
Bansic20	16-25 Sept 2020	G. Dallaporta	11	1000	44	0.596	1.566	0.032	0.697	1.083	0.433	19.861	0.222	38.091	0.0096
Bansic21	6-18 Sept 2021	G. Dallaporta	15	996	67	0.577	1.449	0.073	1.333	1.087	0.526	19.623	0.222	37.822	0.0128

274

Layer 200-500 m															
Bansic10	25 June–14 Jul 2010	Urania	13	700	26	4.086	0.230	0.166	0.462	4.606	0.299	14.155	0.017	38.742	0.0014
Bansic11	08–26 Jul 2011	Urania	34	1130	65	5.400	0.254	0.135	0.425	4.860	0.348	14.196	0.010	38.753	0.0022
Bansic12	04–23 Jul 2012	Urania	39	1711	68	4.407	0.244	0.170	0.342	4.443	0.342	14.336	0.016	38.814	0.0007
Bansic13	26 June–16 Jul 2013	Urania	34	1700	65	4.473	0.216	0.163	0.338	4.623	0.271	14.325	0.017	38.819	0.0006
Bansic14	22 Jul–9 Aug 2014	Urania	32	1700	61	4.753	0.190	0.178	0.299	4.047	0.305	14.474	0.022	38.852	0.0013
Bansic15	16 Jul–3 Aug 2015	Minerva Uno	31	1700	57	2.976	0.402	0.148	0.476	2.589	0.528	14.677	0.020	38.858	0.0014
Bansic16	30 June–14 Jul 2016	Minerva Uno	10	1700	23	4.002	0.277	0.096	0.585	3.097	0.416	14.794	0.022	38.892	0.0007
Bansic17	13–29 June 2017	Minerva Uno	32	1700	52	4.017	0.290	0.167	0.397	4.193	0.294	14.705	0.021	38.900	0.0006
Bansic18	07-19 Sept 2018	G. Dallaporta	16	700	16	4.460	0.142	0.095	0.520	4.223	0.185	14.584	0.018	38.885	0.0006
Bansic19	30 Sept-12 Oct 2019	G. Dallaporta	6	72											
Bansic20	16-25 Sept 2020	G. Dallaporta	11	1000	11	4.301	0.068	0.115	0.171	3.869	0.161	14.464	0.013	38.873	0.0006
Bansic21	6-18 Sept 2021	G. Dallaporta	15	996	13	5.025	0.319	0.204	0.304	4.677	0.254	14.634	0.016	38.872	0.0005

275

Layer 500-bottom															
Bansic10	25 June–14 Jul 2010	Urania	13	700	4	4.420	0.006	0.097	0.339	4.987	0.045	13.908	0.004	38.777	0.0002
Bansic11	08–26 Jul 2011	Urania	34	1130	25	5.861	0.125	0.179	0.280	6.392	0.163	13.946	0.003	38.787	0.0002
Bansic12	04–23 Jul 2012	Urania	39	1711	49	5.413	0.171	0.216	0.217	6.468	0.163	13.997	0.005	38.780	0.0003
Bansic13	26 June–16 Jul 2013	Urania	34	1700	39	4.886	0.158	0.207	0.212	6.474	0.150	14.019	0.003	38.794	0.0002
Bansic14	22 Jul–9 Aug 2014	Urania	32	1700	37	5.546	0.106	0.239	0.190	6.088	0.127	14.069	0.003	38.811	0.0003
Bansic15	16 Jul–3 Aug 2015	Minerva Uno	31	1700	26	4.130	0.240	0.238	0.267	4.701	0.277	14.125	0.003	38.817	0.0003
Bansic16	30 June–14 Jul 2016	Minerva Uno	10	1700	16	5.774	0.240	0.118	0.339	6.180	0.237	14.222	0.006	38.834	0.0005
Bansic17	13–29 June 2017	Minerva Uno	32	1700	25	4.954	0.231	0.241	0.203	6.205	0.117	14.229	0.003	38.837	0.0003
Bansic18	07-19 Sept 2018	G. Dallaporta	16	700	3	5.315	0.036	0.159	0.093	5.905	0.084	14.200	0.003	38.832	0.0003
Bansic19	30 Sept-12 Oct 2019	G. Dallaporta	6	72											
Bansic20	16-25 Sept 2020	G. Dallaporta	11	1000	7	4.650	0.017	0.155	0.070	5.038	0.030	14.201	0.003	38.834	0.0002
Bansic21	6-18 Sept 2021	G. Dallaporta	15	996	7	5.474	0.299	0.241	0.279	6.229	0.191	14.248	0.003	38.815	0.0002

276

277

278

279

280

281

282

283

284

285

286

287

288

289

290

291

292

293

294

295

296

As far as the hydrological properties of the water masses in the study area, it is worth noting that over the (summer) period 2010-2021 in the surface layer the average temperature varied in the range 17.380-19.861 °C, with a general increasing trend peaking in 2020. Similarly, the salinity showed increasing values in the range 37.610-38.206 with a peak of in 2015 (Tab. 2). This layer is characterized by a strong interannual and spatial variability as subject to continuous interaction with the atmosphere, as also highlighted by one or two higher orders of magnitude in CV values of physical parameters in the superficial layer compared to the deeper layers (Fig. 2f, g; Tab. 2). Indeed, in the upper layer the CV of temperature varied between 0.148 (BANSIC10) and 0.240 (BANSIC15), and the CV of salinity ranged between 0.007 (BANSIC19) and 0.014 (BANSIC16).

Instead, the deeper water masses, with their lower variability in heat and salt content turn out to be much more suitable for monitoring any changes over long periods. In the IW layer the CV of temperature ranged between 0.010 (BANSIC11) and 0.022 (BANSIC14 and BANSIC16), while the CV of salinity ranged between 0.0005 (BANSIC21) and 0.0022 (BANSIC11) (Tab. 2). Values of temperature in our time series (2010-2021) shows an increase in average values of about 0.5 °C (14.155-14.634 °C), with a peak of 14.794 in 2017 (Tab. 2). Similarly, the corresponding increase in salinity was about 1.15 psu (37.742-38.885) with a peak of 38.900 psu reached in 2018 (Tab. 2). Similar trends have been also highlighted in the same area by Schroeder et al. (2017) and related to the increase to drying processes affecting the surface waters from which the IW originates. Within

297 the time series (2010-2021) two patterns can be distinguished, the first (2010-2016) is characterized
298 by an average annual increase in temperature (dT/dt) of about $0.1\text{ }^{\circ}\text{C}/\text{year}$, the second one (2017-
299 2020) by an annual decrease in temperature of $0.08\text{ }^{\circ}\text{C}/\text{year}$ (Fig. 2i; Tab. 2). Finally, in 2021 a slight
300 rise in temperature occurred (Fig. 2i; Tab. 2). Similarly, the salinity patterns show an average annual
301 increase (dS/dt) of 0.022 over the period 2010-2016 and an annual decrease of 0.007 afterwards
302 (2017-2021) (Fig. 2i; Tab. 2). A recent study advanced hypotheses on a possible link between the
303 temperature and salinity positive trends over the period 2010-2016 and the anticyclonic phase of
304 the NIG over the years 2006-2010, while the negative trends over the period 2017-2021 have been
305 connected to the cyclonic phase of the NIG during years 2011-2016 (Placenti et al., 2022).
306 Conversely, the nitrates and silicates mean annual concentrations show a slight decrease up to
307 2015-2016 and then slight increase until 2021 (Tab. 2), in agreement with the state of the art
308 regarding the SC (Placenti et al., 2022).
309 The DW are characterized by very low values in CV of both temperature and salinity (between 0.003 -
310 0.006 and 0.002 - 0.005 , respectively) with very slight differences across the yearly surveys (Tab. 2).
311 Moreover, the average annual temperature and salinity slightly increased from 2010 until 2017
312 (13.908 - $14.299\text{ }^{\circ}\text{C}$ and 38.777 - 38.837), and then slightly decreased until 2020 (Tab. 2). On the
313 contrary, the patterns of nitrates and silicates would appear to be characterized by a slight decrease
314 (5.861 - 4.130 and 6.392 - $4.701\text{ }\mu\text{mol/l}$) between 2011 and 2015 and by a slight discontinuous
315 increase afterwards until 2021 (Tab. 2).

316

317 **DATA AVAILABILITY**

318 The final product is available from ZENODO and can be accessed in full open access form at
319 <https://doi.org/10.5281/zenodo.8125006> (Placenti et al., 2023).

320

321 **CONCLUSION**

322 The dataset described here has the advantage of having been collected within the same monitoring
323 program implemented on an important area of the Mediterranean Sea. Over time, the data has
324 been collected consistently by the same technicians and researchers, who have been able to apply
325 a rigorous quality check during both field and laboratory activities. This made it possible to minimize
326 any biases deriving from the different experience of the personnel and from the use of different
327 types of instrumentation and protocols. The spatial and temporal variability that characterizes this
328 dataset therefore reliably reflects the effect of environmental processes that occurred in the marine

329 environment, making this dataset usable for different fields of application. In support to this, the
330 analysis of the mean values and of the variability of the parameters along the water column and
331 among different surveys showed an agreement with the patterns commonly recognized in the
332 marine environment and highlighted in other datasets collected in different areas of the
333 Mediterranean Sea. Moreover, the analysis shown in this paper is highly consistent with the trends
334 evidenced in the literature concerning the Sicily Channel. In this framework, the availability of this
335 dataset to the scientific community fills an important lack in field observations of a crucial area, the
336 Sicily Channel, where exchanges between the western and eastern Mediterranean basin take place,
337 providing support to studies aimed at describing the ongoing processes as well as at realizing reliable
338 projections regarding the effects of these processes in the near future.

339

340 **AUTHOR CONTRIBUTIONS**

341 FP wrote the manuscript and analyzed the dataset. MT wrote the manuscript and prepared the
342 figures. VT and CB participated to the fieldwork and laboratory analyses. KS wrote the manuscript
343 and improved the quality check of the oceanographic data. GC, AC and BP coordinated the field
344 work and the laboratory analyses and supervised the writing of the text. MB managed the technical
345 aspects related to the oceanographic instrumentation for the acquisition of the hydrological
346 parameters and helped with specific technical aspects of the manuscript. All authors contributed to
347 the article and approved the submitted version.

348

349 **COMPETING INTERESTS**

350 The authors declare that they have no conflict of interest.

351

352 **FINANCIAL SUPPORT**

353 This study was mainly supported by the Italian National Research Council (CNR) through USPO office
354 and by the FAO Regional Project MedSudMed “Assessment and Monitoring of the Fishery Resources
355 and the Ecosystems in the Straits of Sicily”, co-funded by the Italian Ministry MIPAAF through the
356 Directorate General for Maritime Affairs and Fisheries of the European Commission (DG MARE).
357 Other national research programmes supported this study including project SSD-PESCA,
358 coordinated by the Ministry of the Education, University and Research (MIUR) and founded by the
359 Ministry of Economic Development (MISE), and the Flagship Project RITMARE – The Italian Research
360 for the Sea, coordinated by the Italian National Research Council and funded by MIUR.

361

362 **ACKNOWLEDGMENTS**

363 Masters of the Urania, Minerva Uno, Dallaporta and all their crew are thanked for their work in
364 support to the sampling activities during the oceanographic cruises. We are grateful to Carmelo
365 Bennici, Girolama Biondo, Gaspare Buffa, Ignazio Fontana, Giovanni Giacalone, Luigi Giaramita,
366 Marianna Musco, Carlo Patti and Giorgio Tranchida for their valuable technical support and the
367 sampling collection during the oceanographic surveys.

368

369 **REFERENCES**

370

371 Belgacem, M., Chiggiato, J., Borghini, M., Pavoni, B., Cerrati, G., Acri, F., Cozzi, S., Ribotti, A., Álvarez,
372 M., Lauvset, S. K., and Schroeder, K.: Dissolved inorganic nutrients in the western
373 Mediterranean Sea (2004–2017), *Earth Syst. Sci. Data*, 12, 1985–2011, 2020,
374 <https://doi.org/10.5194/essd-12-1985-2020>, 2020.

375 Ben Ismail, S., Schroeder, K., Sammari, C., Gasparini, G. P., Borghini, M., and Aleya, L.: Interannual
376 variability of water mass properties in the Tunisia-Sicily Channel, *J. Mar. Syst.*, 135, 14–28,
377 2014.

378 Bonanno, A., Placenti, F., Basilone, G., Mifsud, R., Genovese, S., Patti, B., Di Bitetto, M., Aronica, S.,
379 Barra, M., Giacalone, G., Ferreri, R., Fontana, I., Buscaino, G., Tranchida, G., Quinci E., and
380 Mazzola, S.: Variability of water mass properties in the Strait of Sicily in summer period of
381 1998–2013, *Ocean Sci.* 10:759–770, 2014.

382 Borghini, M., Bryden, H., Schroeder, K., Sparnocchia, S., and Vetrano, A.: The Mediterranean is
383 becoming saltier, *Ocean Sci.* 10, 693–700, <http://dx.doi.org/10.5194/os-10-693-2014>, 2014.

384 Gačić, M., Schroeder, K., Civitarese, G., Cosoli, S., Vetrano, A., and Borzelli, G.L.E.: Salinity in the Sicily
385 channel corroborates the role of the Adriatic-Ionian bimodal oscillating system (BiOS) in
386 shaping the decadal variability of the Mediterranean overturning circulation, *Ocean Sci.* 9, 83–
387 90, <https://doi.org/10.5194/os-9-83-2013>, 2013.

388 Gasparini, G.P., Ortona, A., Budillon, G., Astraldi, M., and Sansone, E.: The effect of the Eastern
389 Mediterranean Transient on the hydrographic characteristics in the Strait of Sicily and in the
390 Tyrrhenian Sea, *Deep-Sea Res. I Oceanogr. Res. Pap.* 52 (6), 915–935, 2005.

391 Grasshoff, K., Kremling, K., and Ehrhardt, M.: *Methods of Seawater Analysis*. Wiley-Vch Verlag,
392 Weinheim, 1999.

393 Hansen, H. P. and Koroleff, F.: Determination of nutrients, *Methods of Seawater Analysis*, 10, 159–
394 228, 1999.

395 Huertas, I.E., Rios, A.F., Garcia-Lafuente, J., Navarro, G., Makaoui, A., Sanchez-Roman, A., Rodriguez-
396 Galvez, S., Orbi, A., Ruiz, J., and Perez, F.F.: Atlantic forcing of the Mediterranean oligotrophy,
397 *Glob. Biogeochem. Cycles* 26, GB2022, <http://dx.doi.org/10.1029/2011GB004167>, 2012.

398 Krom, M.D., Woodward, E.M.S., Herut, B., Kress, N., Carbo, P., Mantoura, R.F.C., Spyres, G.,
399 Thingstad, T.F., Wassmann, P., Wexels Riser, C., Kitidis, V., Law, C.S., and Zodiatis, G.: Nutrient
400 cycling in the south east Levantine basin of the Eastern Mediterranean: results from a
401 phosphorus starved system, *Deep-Sea Res. II* 52 (22–23), 2879–2896, 2005.

402 Krom, M. D., Emeis, K. C., and Van Cappellen, P.: Why is the eastern Mediterranean phosphorus
403 limited? *Prog. Oceanogr.*, 85(3–4), 236–244, [http://dx.doi.org/10.1016/j.pocean.2010.](http://dx.doi.org/10.1016/j.pocean.2010.03.003)
404 03.003, 2010.

405 Placenti, F., Schroeder, K., Bonanno, A., Zgozi, S., Sprovieri, M., Borghini, M, Rumolo, P., Cerrati, G.,
406 Bonomo, S., Genovese, S., Basilone, G., Haddoud, D. A., Patti, B., El Turki, A., Hamza, M., and
407 Mazzola, S.: Water masses and nutrient distribution in the Gulf of Syrte and between Sicily
408 and Libya, *J. Marine Sys.*, 121–122, 36–46, 2013, [http://dx.doi.org/10.1016/j.imarsys.2013](http://dx.doi.org/10.1016/j.imarsys.2013.03.012)
409 [.03.012](http://dx.doi.org/10.1016/j.imarsys.2013.03.012), 2013.

410 Placenti, F., Torri, M., Pessini, F., Patti, B., Tancredi, V., Cuttitta, A., Giaramita, L., Tranchida, G., and
411 Sorgente, R.: Hydrological and biogeochemical patterns in the Sicily Channel: new insights
412 from the last decade (2010-2020), *Front. Mar. Sci.* 9, [https://doi.org/10.3389/fmars.2022.](https://doi.org/10.3389/fmars.2022.733540)
413 [733540](https://doi.org/10.3389/fmars.2022.733540), 2022.

414 Placenti, F., Torri, M., Borghini, M., Cerrati, G., Cuttitta, A., Tancredi, V., Buscaino, C., and Patti,
415 Bernardo. New hydrological-biogeochemical dataset (2010-2021) in the Strait of Sicily [Data
416 set and metadata]. Zenodo. <https://doi.org/10.5281/zenodo.8125006>, 2023.

417 Powley, H.R., Krom, M.D., and Van Cappellen, P.: Understanding the unique biogeochemistry of the
418 Mediterranean Sea: insights from a coupled phosphorus and nitrogen model *Glob.*
419 *Biogeochem. Cycles*, 31, pp. 1010-1031, 10.1002/2017GB005648, 2017.

420 Redfield, A.C., Ketchum, B.H., and Richards, F.A.: The influence of organisms on the composition of
421 sea water, In: Hill, M.N. (Ed.), *The Sea*, vol. 2. Interscience, New York, pp. 224–228, 1963.

422 Ribera D'Alcalà, M., Civitarese, G., Conversano, F., and Lavezza, R.: Nutrient ratios and fluxes hint at
423 overlooked processes in the Mediterranean Sea, *J. Geophys. Res.*,108(C9),8106,
424 doi:10.1029/2002JC0016500, 2003.

425 Roether, W., Manca, B.B., Klein, B., Bregant, D., Georgopoulos, D., Beitzel, V., Kovacević, V., and
426 Luchetta, A.: Recent changes in eastern mediterranean deep waters, *Science* 271 (5247), 333–
427 335, <http://dx.doi.org/10.1126/science>, 1996.

428 Schroeder, K., Gasparini, G. P., Borghini, M., Cerrati, G., and Delfanti, R.: Biogeochemical tracers and
429 fluxes in the Western Mediterranean Sea, spring 2005, *J. Mar. Syst.* 80, 8–24, doi:
430 10.1016/j.jmarsys.2009.08.002, 2010.

431 Schroeder, K., Chiggiato, J., Josey, S. A., Borghini, M., Aracri, S., and Sparnocchia, S.: Rapid response
432 to climate change in a marginal sea. *Sci. Rep.* 7:4065, doi: 10.1038/s41598-017-04455-5, 2017.

433 Schroeder, K., Chiggiato, J., Ben Ismail, S., Borghini, M., Patti, B. and Sparnocchia, S.: Mediterranean
434 deep and intermediate water mass properties. In: Copernicus Marine Service Ocean State
435 Report, Issue 3, *Journal of Operational Oceanography*, 12:sup1, s26–s30; doi:
436 10.1080/1755876X.2019.16330, 2019.

437 Sorgente, R., Olita, A., Oddo, P., Fazioli, L., and Ribotti, A.: Numerical simulation and decomposition
438 of kinetic energy in the Central Mediterranean: insight on mesoscale circulation and energy
439 conversion, *Ocean Sci.*, 7, 503–519, doi: 10.5194/os-7-503-2011, 2011.

440 The Mermex group: Durrieu de Madron, X., Guieu, C., Sempéré, R., Conan, P., Cossa, D., D’Ortenzio,
441 F., Estournel, C., Gazeau, F., Rabouille, C., Stemmann, L., Bonnet, S., Diaz, F., Koubbi, P.,
442 Radakovitch, O., Babin, M., Baklouti, M., Bancon-Montigny, C., Belviso, S., Bensoussan, N.,
443 Bonsang, B., Bouloubassi, I., Brunet, C., Cadiou, J.-F., Carlotti, F., Chami, M., Charmasson, S.,
444 Charrière, B., Dachs, J., Doxaran, D., Dutay, J.-C., Elbaz-Poulichet, F., Eléaume, M., Eyrolles, F.,
445 Fernandez, C., Fowler, S., Francour, P., Gaertner, J.C., Galzin, R., Gasparini, S., Ghiglione, J.-F.,
446 Gonzalez, J.-L., Goyet, C., Guidi, L., Guizien, K., Heimbürger, L.-E., Jacquet, S.H.M., Jeffrey,
447 W.H., Joux, F., Le Hir, P., Leblanc, K., Lefèvre, D., Lejeusne, C., Lemé, R., Loÿe-Pilot, M.-
448 D., Mallet, M., Méjanelle, L., Mélin, F., Mellon, C., Mérigot, B., Merle, P.-L., Migon, C., Miller,
449 W.L., Mortier, L., Mostajir, B., Mousseau, L., Moutin, T., Para, J., Pérez, T., Petrenko, A.,
450 Poggiale, J.-C., Prieur, L., Pujo-Pay, M., Pulido-Villena, Raimbault, P., Rees, A.P., Ridame, C.,
451 Rontani, J.-F., Ruiz Pino, D., Sicre, M.A., Taillandier, V., Tamburini, C., Tanaka, T., Taupier-
452 Letage, I., Tedetti, M., Testor, P., Thébault, H., Thouvenin, B., Touratier, F., Tronczynski, J.,
453 Ulses, C., Van Wambeke, F., Vantrepotte, V., Vaz, S., Verney, R.: Marine ecosystems’ responses
454 to climatic and anthropogenic forcings in the Mediterranean, *Prog. Oceanogr.*, 91.
455 doi:10.1016/j.pocean.2011.02.003.T, 2011.

456 SeaDataNet: Data Quality Control Procedures, 6th Framework of EC DG Research, Version 2.0, May
457 2010, <https://www.seadatanet.org/Standards/Data-Quality-Control>, 2010

458 Stansfield, K., Gasparini, G.P., and Smeed, D.A.: High-resolution observations of the path of the
459 overflow from the Sicily Strait, *Deep Sea Res., Part I*, 50, 1129–1149, 2003.

460 Van Cappellen, P., Powley, H. R., Emeis, K.-C., and Krom, M. D.: A biogeochemical model for
461 phosphorus and nitrogen cycling in the eastern Mediterranean Sea (EMS), Part 1. Model
462 development, initial conditions and sensitivity analyses, *J. Mar. Syst.*, 139, 460–471, 2014.